RSC Advances

PAPER

View Article Online
View Journal | View Issue

Cite this: *RSC Adv.*, 2025, **15**, 38014

Enzymatic, cell-based, and *in silico* evaluation of di-substituted aminomethyl-1,2,3-triazole–cinamamide hybrids as mushroom tyrosinase inhibitors

Navid Dastyafteh,[a] Mohammad Hosein Sayahi,[b] Mohammad Hossein Morshedsolouk,[c] Sajedeh Safapoor,[c] Mohammad Mahdavi,[c] Mina Saeedi,[de] Haleh Hamedifar,[fg] Nima Sepehri*[fg] and Aida Iraji *[ah]

A series of novel aryl-substituted aminomethyl 1,2,3-triazole–cinamamide hybrids (**9a–q**) were synthesized and tested as tyrosinase inhibitors using enzymatic, *in silico*, and cell-based assays. A multi-step synthetic procedure, involving coupling *N*-(prop-2-yn-1-yl)cinnamamide intermediates with various azido-functionalized anilide derivatives and click chemistry, gives the final 1,2,3-triazole-linked hybrids in good yields. SAR studies pointed out that compound **9i** (R^1 = 4-Cl, R^2 = 4-Br) was the best tyrosinase inhibitor and was found to be a promising antioxidant in DPPH radical scavenging (51.82% at 200 μM). Kinetic studies on the enzyme reveal that the inhibition type is competitive with a K_i value of 34.36 μM. Further molecular docking and molecular dynamics simulations supported the strong binding interaction of **9i** in the tyrosinase active site *via* π–π stacking interactions with the His residues and hydrogen bonding with important catalytic residues. Consistent with these findings, *in vitro* studies showed that **9i** had low cytotoxicity to B16F10 melanoma cells at concentrations ≤100 μM but was able to reduce intracellular melanin content from 92 to 62 μg mL^{-1}. Therefore, compound **9i** represents a potent tyrosinase inhibitor with antioxidant and anti-melanogenic properties, which might further assist in the development of anti-melanoma agents.

Received 18th June 2025
Accepted 11th September 2025

DOI: 10.1039/d5ra04315h

rsc.li/rsc-advances

1. Introduction

Tyrosinase (polyphenol oxidase, EC 1.14.18.1) is a multifunctional copper-containing enzyme found in various organisms, from bacteria to plants to animals. It is a very important enzyme in melanin biosynthesis since it hydroxylates L-tyrosine to L-DOPA (3,4-dihydroxyphenylalanine) and then oxidizes L-DOPA to dopaquinone, a principal precursor in melanin synthesis.[1] The enzyme is crucial for skin pigment formation and causes enzymatic browning in plants and cuticle formation in insects. Overactivation in tyrosinase activity leads to hyperpigmentation disorders, such as melasma, age spots, and post-inflammatory hyperpigmentation, which seriously mar the cosmetic appeal of patients and resultant psychological trauma.[2,3] While atypical melanin production is associated with the exacerbation of melanoma, tyrosinase inhibitors could aid in treating skin cancers. Furthermore, more recent studies point toward possible roles tyrosinase may play in neurodegenerative disorders such as Parkinson's, where dopamine metabolism is impaired.[4]

In the food industry, tyrosinase-mediated enzymatic browning occurs, leading to deteriorating quality in fruits, vegetables, and seafood.[5] Browning destroys visual appeal and, by extension, depletes nutritional potential through the degradation of active compounds and vitamins. Traditional inhibitors such as sulfites and ascorbic acid have been limited by regulatory restrictions and inconsistent efficiency.[6] Thus, a novel tyrosinase inhibitor, whether natural or synthetic, should be identified with a better safety profile and improved stability for food preservation and extended shelf life.

Cinnamic acid (**A**, Fig. 1) and its derivatives are regarded as potent tyrosinase inhibitors, due to their resemblance to

[a]*Stem Cells Technology Research Center, Shiraz University of Medical Sciences, Shiraz, Iran. E-mail: aida.iraji@gmail.com; iraji@sums.ac.ir*
[b]*Department of Chemistry, Payame Noor University, Tehran, Iran*
[c]*Endocrinology and Metabolism Research Center, Endocrinology and Metabolism Clinical Sciences Institute, Tehran University of Medical Sciences, Tehran, Iran*
[d]*Persian Medicine and Pharmacy Research Center, Tehran University of Medical Sciences, Tehran, Iran*
[e]*Medicinal Plants Research Center, Faculty of Pharmacy, Tehran University of Medical Sciences, Tehran, Iran*
[f]*CinnaGen Medical Biotechnology Research Center, Alborz University of Medical Sciences, Karaj 1461965381, Iran. E-mail: N.sepehri@nanoalvand.com*
[g]*CinnaGen Research and Production Co., Alborz 3164819712, Iran*
[h]*Research Center for Traditional Medicine and History of Medicine, Department of Persian Medicine, School of Medicine, Shiraz University of Medical Sciences, Shiraz, Iran*

tyrosine, the enzyme's natural substrate. The presence of this α,β-unsaturated carbonyl moiety renders these compounds competitive inhibitors, targeting the enzyme's active site.[7] Substitution on the phenyl ring with hydroxyl or methoxy groups has been reported to improve inhibitory activity greatly . *p*-Coumaric acid (**B**, Fig. 1) was found to be more potent than cinnamic acid, probably due to the extra hydrogen bonding with the enzyme.[8] Likewise, ferulic acid has been reported to exert a very strong anti-melanogenic effect on B16F10 melanoma cells, suggesting it could have applications in cosmetics and therapeutics.[9] Caffeic acid (3,4-dihydroxycinnamic acid, **C**, Fig. 1), being more active than mono-substituted derivatives, presumably chelates copper better at the enzyme active site.[10] Nonetheless, some cinnamic acid derivatives are limited in use due to their poor stability under UV light; thus, hybrid molecules with better properties are being investigated.

Amino 1,2,3-triazoles (**D–F**, Fig. 1) have always been of interest as tyrosinase inhibitors. Different reports on this particular class of compounds have pointed out their ability to form coordination complexes with copper ions at the active site of the enzyme.[11,12] In recent decades, researchers have put much effort into modifying the 1,2,3-triazole scaffold to achieve selective and potent action against tyrosinase.[13–15]

Hybrid molecules with phenolic moieties conjugated to 1,2,3-triazoles showed better inhibition. Drug design efforts have recently investigated hybrid molecules combining a cinnamic acid and 1,2,3-triazole pharmacophore (**G**, Fig. 1) as a tyrosinase inhibitor. In the enzymatic assays, the most potent compound showed around 45% inhibition at 40 μM. SAR studies on this hybrid halogen, because of their electron-withdrawing nature, enhance inhibition of tyrosinase by stabilizing the enzyme–inhibitor complex, and electron donors at the ortho position tend to enhance inhibition as well.[16]

As a result of the current study, cinnamic derivatives mimicking the natural substrate, L-tyrosine, and the 1,2,3-triazole moiety, which enhances binding affinity with the enzyme active site, were selected as the primary backbone. The design strategy involves optimizing the cinnamic ring (R^1) with different groups as well as modifying the 1,2,3-triazole (R^2) with flexible linkers. *In vitro* assays, cell toxicity, and melanin determination in B16F10 cells, along with molecular docking

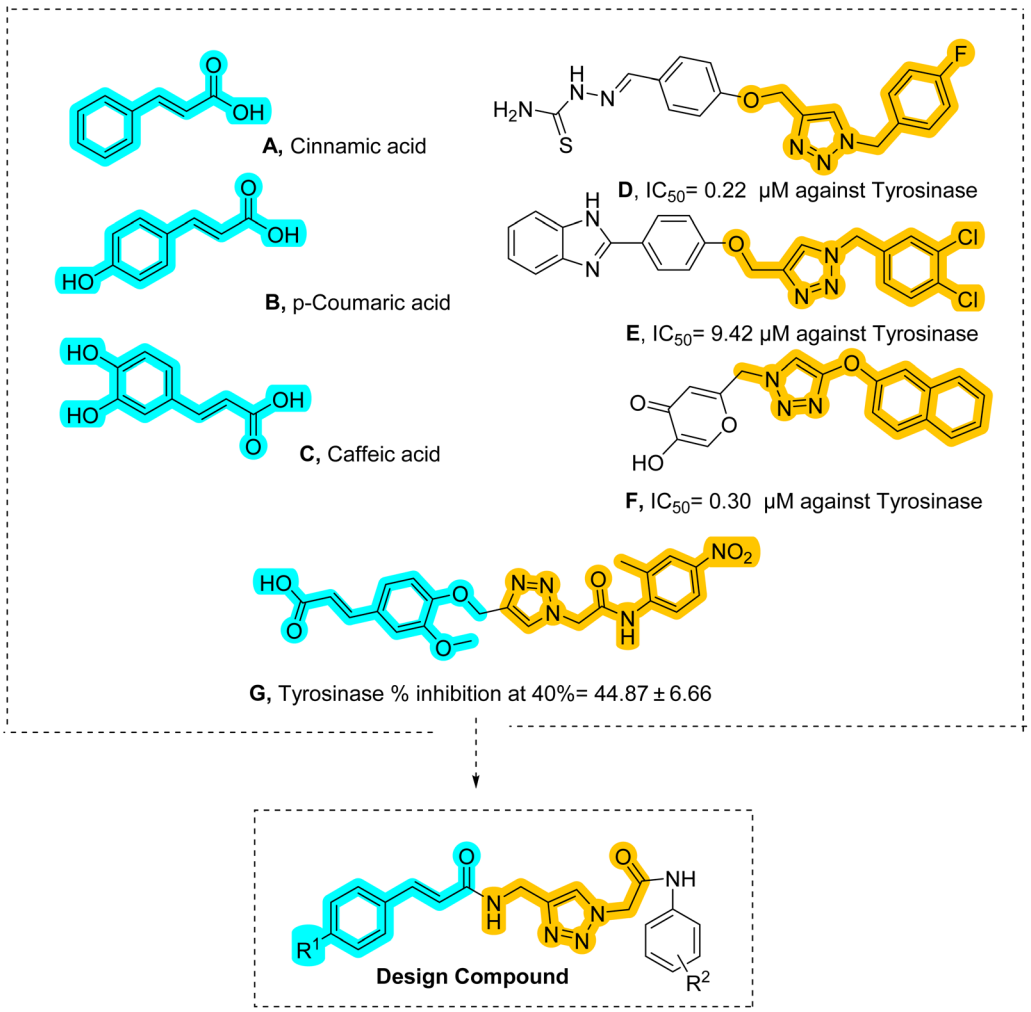

Fig. 1 Designing.

and molecular dynamics simulations, were conducted to predict key interactions.

2. Results and discussion

2.1 Chemistry

A mixture containing benzaldehyde derivatives **1a–c**, malonic acid, pyridine, and piperidine as a catalyst was stirred at 100 °C for 3 hours. Afterward, water was added, and the mixture was neutralized with concentrated HCl, yielding cinnamic acid derivatives **3a–c**. To a solution of cinnamic acid derivatives **3a–c** and propargylamine **4** in DMF, TBTU and Et_3N were added. The mixture was stirred at room temperature for 24 hours. Upon completion of the reaction, water was added, and the resulting precipitate was filtered to obtain pure *N*-(prop-2-yn-1-yl) cinnamamide derivatives **5a–c**. Aniline derivatives **6a–f** were suspended in DMF and cooled to 0 °C. Chloroacetyl chloride was then added, and the reaction mixture was stirred at room temperature for 24 hours. After completion, the mixture was diluted with water, poured over crushed ice, and the resulting precipitate was filtered. The residue was washed with water to obtain 2-chloro-*N*-substituted acetamide derivatives **7a–f**. Next, **7a–f**, K_2CO_3, and NaN_3 were dissolved in DMF and stirred at room temperature for 1 hour. According to Sharpless and co-workers' report for regioselective synthesis, 1,4-disubstituted 1,2,3-triazoles were obtained by the addition of copper sulfate pentahydrate ($CuSO_4 \cdot 5H_2O$), sodium ascorbate, and *N*-(prop-2-yn-1-yl)cinnamamide derivatives **5a–c**.[17] Upon completion of the reaction, copper ions were removed using an EDTA solution. The resulting precipitate was filtered, washed several times with water, and crystallized from ethyl acetate to yield pure *N*-((1*H*-1,2,3-triazol-4-yl)methyl)cinnamamide-*N*-substituted acetamides **9a–q** (Scheme 1).

The structures of the synthesized compounds were elucidated using NMR and IR spectroscopy. The purity of compound **9i** was confirmed using HPLC, and compound **9q** was further characterized using high-resolution mass spectrometry (HRMS), which provided accurate mass data supporting its structural assignment.

2.2 Structure–activity relationship (SAR) analysis of 9a–p against tyrosinase

The SAR analysis of these compounds reveals clear trends that depend on the R^1 and R^2 substitutions. The parent compound **9a**, where R^2 is hydrogen, is almost inactive (IC_{50} > 200 μM). The incorporation of 4-F on R^2 (**9b**) enhances the potency (IC_{50} = 158.53 μM), whereas 4-Cl (**9c**) has moderate potency (IC_{50} = 190.76 μM); the best activity within the set returned to 4-Br (**9d**) with IC_{50} = 142.56 μM. The 4-ethyl group (**9e**) offers the same moderate improvement (IC_{50} = 178.23 μM), as electron-withdrawing at R^2 enhances activity compared to the unsubstituted analog **9a**, but is not enough to achieve strong inhibition.

The substitution of R^1 with 4-Cl (**9f–k**) is associated with an overall enhancement of the activity relative to the R^1=H set. The parent R^2-unsubstituted compound (**9f**) shows intermediate potency (IC_{50} = 153.03 μM), and the introduction of 4-F to R^2 (**9g**) enhances the activity (IC_{50} = 138.37 μM). Significantly, the introduction of 4-Cl at both R^1 and R^2 (**9h**) leads to the loss of potency (IC_{50} > 200 μM), indicating steric hindrance and/or electronic repulsion. The optimal compound in the set is **9i** (R^1 = 4-Cl, R^2 = 4-Br), which is the most active (IC_{50} = 66.23 μM), followed by **9j** (R^2 = 4-ethyl, IC_{50} = 96.32 μM). This indicates that bulkier or more polarizable R^2 substituents, such as 4-Br, greatly increase the activity in the set. Compound **9k** bearing a 4-MeO substituent showed markedly reduced potency, with IC_{50} > 200 μM, indicating that heteroatom-based electron-donating substitution is not beneficial.

In the case of the R^1 = 4-MeO derivatives (**9l–q**), the trend is as expected with moderate activity across various R^2 substituents. The parent compound (**9l**) showed an IC_{50} of 165.57 μM with improvements seen in 4-F (**9m**, IC_{50} = 158.56 μM), 4-Cl (**9n**,

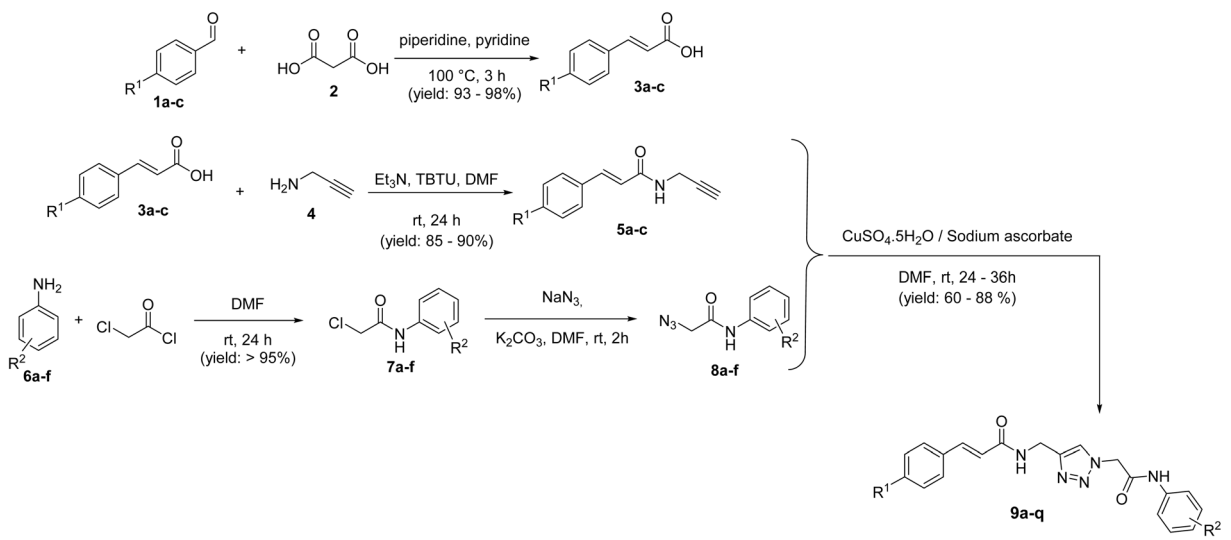

Scheme 1 Synthesis of **9a–q**.

IC_{50} = 148.01 μM), and 4-Br (**9o**, IC_{50} = 139.48 μM). The 4-ethyl substituent (**9p**) affords an IC_{50} of 153.15 μM.

Compound **9q** bearing MeO substitution at R^1 and R^2 shows IC_{50} = 182.86 ± 5.54, so that such bulk electron donating does not improve the potency *vs.* **9i**.

Overall, SAR trends indicate that the type of substitution at R^2 has a significant impact on activity. The most active compound, **9i** (R^1: 4-Cl, R^2: 4-Br), highlights the critical role of halogen-mediated interactions in increasing potency. The introduction of electron-withdrawing groups at R^2, such as 4-F and 4-Cl, results in moderate potency. In contrast, the 4-Br substituent leads to increased activity, likely due to its bulk and polarizability. Furthermore, evaluations of the nature of the substitution at R^1 indicated that chlorine was superior to unsubstitution and MeO substitution at R^1 (Table 1).

2.3 Antioxidant activity potential

The synthesized compounds are tested for their antioxidant activity *via* the DPPH radical scavenging at 200 μM. The effect of substituents at R^1 or R^2 positions on the % inhibition of DPPH radicals was studied to understand SAR. Quercetin, as a positive control, showed IC_{50} = 18.56 ± 2.19 μM.

Compound **9a** (R^1: H, R^2: H) exhibited the lowest inhibition (23.64%). The introduction of fluorine into the R^2 position (**9b**; R^1: H, R^2: 4-F) caused a notable increase in the antioxidant capacity (64.18%). Substitution with bromine at R^2 (**9d**; R^1: H, R^2: 4-Br) showed a moderate result (41.09%), while chlorine at R^2 (**9c**, R^1: H, R^2: 4-Cl) showed a slightly lower effect (36.91%).

Table 1 Tyrosinase inhibitory activities of **9a–q**[a]

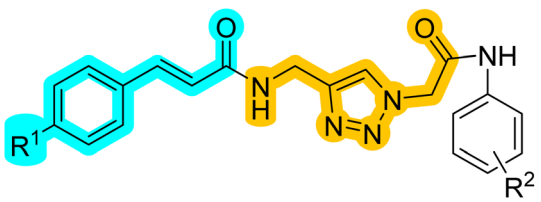

Compound	R^1	R^2	IC_{50} μM
9a	H	H	> 200
9b	H	4-F	158.53 ± 5.16
9c	H	4-Cl	190.76 ± 0.31
9d	H	4-Br	142.56 ± 0.46
9e	H	4-Ethyl	178.23 ± 11.89
9f	4-Cl	H	153.03 ± 7.72
9g	4-Cl	4-F	138.37 ± 13.49
9h	4-Cl	4-Cl	> 200
9i	4-Cl	4-Br	66.23 ± 6.46
9j	4-Cl	4-Ethyl	96.32 ± 4.55
9k	4-Cl	4-MeO	> 200
9l	4-MeO	H	165.57 ± 11.04
9m	4-MeO	4-F	158.56 ± 6.71
9n	4-MeO	4-Cl	148.01 ± 7.71
9o	4-MeO	4-Br	139.48 ± 0.68
9p	4-MeO	4-Ethyl	153.15 ± 18.65
9q	4-MeO	4-MeO	182.86 ± 5.54

[a] Kojic acid as positive control showed IC_{50} = 27.56 ± 1.27 μM.

Table 2 The antioxidant potential of **9a–q**[a]

Compound	R^1	R^2	% Inhibition at 200 μM
9a	H	H	23.64 ± 4.63
9b	H	4-F	64.18 ± 2.31
9c	H	4-Cl	36.91 ± 0.51
9d	H	4-Br	41.09 ± 4.11
9e	H	4-Ethyl	47.36 ± 1.93
9f	4-Cl	H	46.18 ± 1.54
9g	4-Cl	4-F	45.73 ± 3.47
9h	4-Cl	4-Cl	22.82 ± 0.90
9i	4-Cl	4-Br	51.82 ± 2.31
9j	4-Cl	4-Ethyl	82.36 ± 5.91
9k	4-Cl	4-MeO	55.28 ± 0.16
9l	4-MeO	H	43.91 ± 4.50
9m	4-MeO	4-F	60.18 ± 6.94
9n	4-MeO	4-Cl	68.64 ± 7.33
9o	4-MeO	4-Br	57.09 ± 6.17
9p	4-MeO	4-Ethyl	40.73 ± 5.91
9q	4-MeO	4-MeO	61.51 ± 3.74

[a] Quercetin as positive control; IC_{50} = 18.56 ± 2.19 μM.

Among compounds with R^1 = 4-Cl, the presence of 4-Br at R^2 (**9i**) and 4-ethyl at R^2 (**9j**) resulted in increased activity. Compound **9j** (R^1: 4-Cl, R^2: 4-ethyl) exhibited the highest inhibition (82.36%), indicating that the presence of both a chlorine

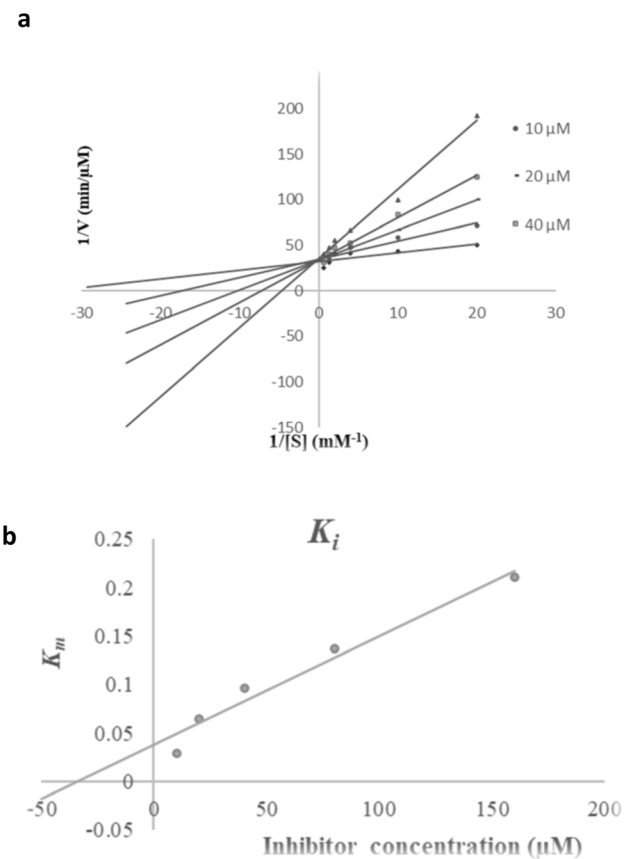

Fig. 2 Kinetics of tyrosinase inhibition by **9i**. (a) The Lineweaver–Burk plot at different concentrations of **9i**; (b) the secondary plot between K_m and various concentrations of **9i**.

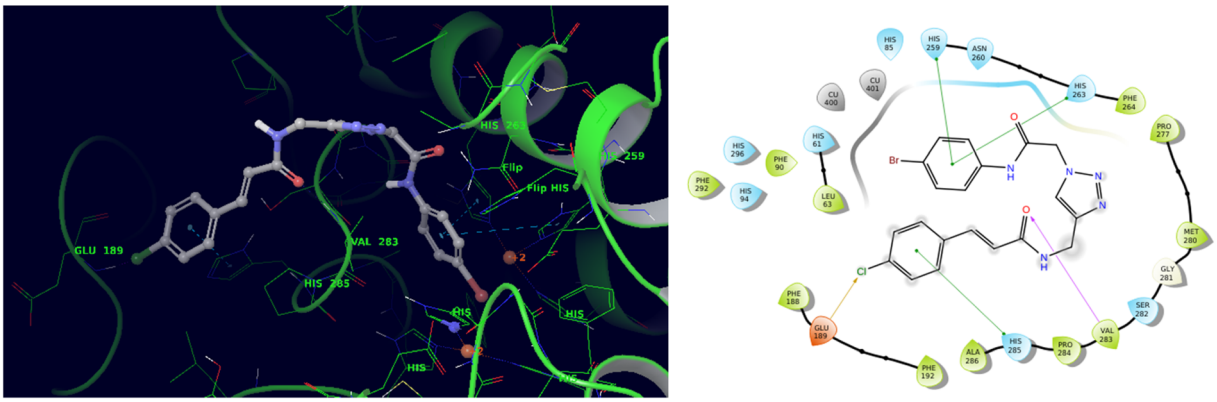

Fig. 3 3D and 2D interaction pattern of **9i** within the active site of tyrosinase.

at R^1 and an ethyl group at R^2 significantly enhances activity. **9k** bearing 4-MeO also exhibited good antioxidant activity with 55.28 ± 0.16% inhibition. A methoxy (–OMe) substitution at R^1 (**9l–q**) enhanced antioxidant activity compared to hydrogen (**9a**). Among these, **9n** (R^1: 4-MeO, R^2: 4-Cl) exhibited the highest activity (68.64%). The combination of 4-MeO at R^1 with halogens at R^2 (**9m**: R^2: 4-F, 60.18%; **9n**: R^2: 4-Cl, 68.64%; **9o**: R^2: 4-Br, 57.09%) improved antioxidant properties. The presence of two methoxy groups in compound **9q** was also beneficial, resulting in 61.51% inhibition.

The overall trend is that an electron-withdrawing group, especially halogens such as fluorine and bromine, at R^2 enhances radical scavenging, and at R^2, bulky alkyl groups such as ethyl considerably enhance the activity. However, the best free radical scavenging activity was accounted for compound **9j** (4-Cl, 4-ethyl) with 82.36% free radical scavenging. Also, the methoxy substitution at R^1 facilitates improved activity, particularly with halogens at R^2, whereas the lowest activity was recorded with those lacking substituents or having excessive halogenation, such as **9h** (R^1: 4-Cl, R^2: 4-Cl) (Table 2).

2.4 Enzyme kinetic studies

To gain insight into the mechanism of action of **9i** as the most potent tyrosinase inhibitor, kinetic measurements were performed. According to Fig. 2a, the Lineweaver–Burk plot showed that K_m gradually increased and V_{max} remained unchanged with increasing inhibitor concentration, indicating competitive inhibition. The results show **9i** interacts with the active site on the enzyme and competes with the substrate for binding to the active site. Furthermore, the plot of the K_m *versus* different concentrations of inhibitor gave an estimate of the inhibition constant, K_i of 34.36 μM (Fig. 2b).

2.5 Molecular docking and molecular dynamics study

To provide docking studies, an initial validation was performed. As a result, tropolone, the co-crystallized ligand, which is an established tyrosinase inhibitor, was docked into the tyrosinase active site. The Root Mean Square Deviation (RMSD) value between the docked pose and the crystallographic conformation was less than 2.0 Å, which confirms that the docking protocol is valid.

Accordingly, molecular docking was performed to understand the binding pose and key interactions of compound **9i**. The most potent compound demonstrated a docking energy of −8.082 kcal mol^{-1}. As can be seen in Fig. 3, the 4-chlorophenyl group of **9i** underwent π–π stacking interactions with His285, an important residue in the enzyme's active site. Conversely, the halogen bond was made with Glu189. The carbonyl oxygen of the cinnamic moiety formed a hydrogen bonding interaction with Val283. On the opposite side of the molecule, the 4-bromophenyl group engaged in two π–π stacking interactions with His263 and His259, both of which are known to be important residues for catalytic activity.

A molecular dynamics study was performed to compare the stability of the tyrosinase in complex with compound **9i** against tyrosinase in its unbound state (Fig. 4). The RMSD of backbone atoms served as an indicator of stability for both systems. As illustrated in Fig. 4, the RMSD of **9i**/tyrosinase was significantly lower (RMSD = 1 Å) compared to tyrosinase enzyme (RMSD = 2 Å), indicating stability of the complex over the 100 ns simulation.

The Root Mean Square Fluctuation (RMSF) plots of the protein were analyzed to assess the mobility and fluctuation of

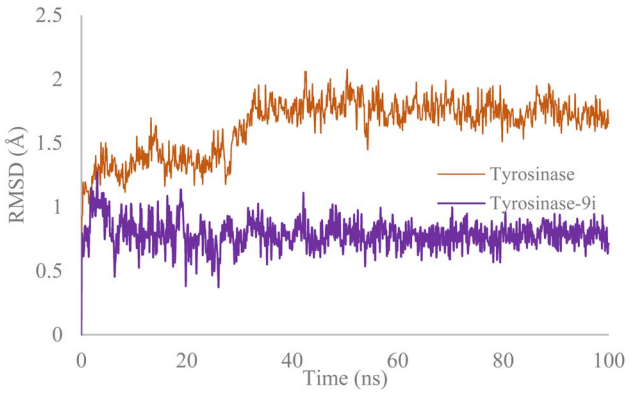

Fig. 4 Superimposed RMSD of Cα atoms of tyrosinase in complex with compound **9i** (purple) and tyrosinase (orange).

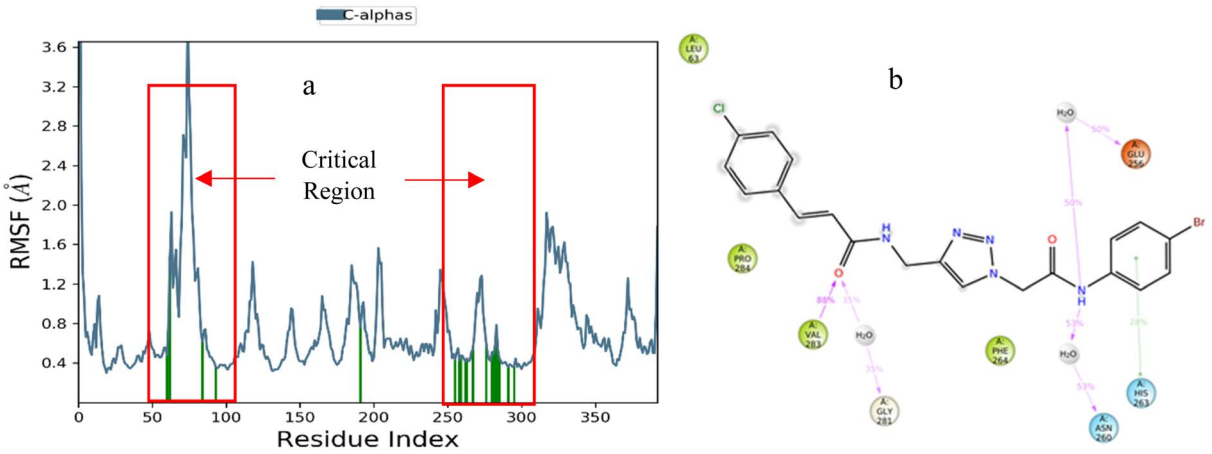

Fig. 5 (a) RMSF of tyrosinase in complex with **9i** (red). (b) Provides a schematic of detailed ligand interactions with protein residues occurring more than 30.0% of the simulation time.

the protein's structure (Fig. 5a). The RMSF of **9i**-tyrosinase enzyme exhibited low fluctuations at residues 59–97 and 254–297, known as the active site region. The interaction between the tyrosinase and the **9i** ligand is visually represented in Fig. 5b, where these interactions were observed during MD simulation. The 4-bromophenyl amine moiety exhibited two hydrogen bonding interactions with Glu256 and Asn260 mediated with water, plus a π–π stacking interaction with His263 (also observed in molecular docking). Additionally, the cinnamic moiety also recorded one direct H-bonding interaction with Val293 and another with Val281, mediated by water (Fig. 5b).

2.6 Cell viability

Compound **9i**, the compound that showed the most potent tyrosinase inhibitory activity, was then evaluated for cytotoxicity in the invasive melanoma B16F10 cells. The cells were then treated with varying concentrations of **9i**, and their viability was assessed using the MTT assay. Concentrations below 100 μM were considered safe based on the melanin content assay (Table 3). At 100 μM, **9i** maintained more than 80% viability, which indicates that this concentration is likely to be low in cytotoxicity.

2.7 Melanin content assay

The effect of the most potent tyrosinase inhibitors on melanin content was analyzed in B16F10 melanoma cells. A melanin calibration curve was first plotted to find the concentration of melanin. Results showed that the untreated control cells produced 92 μg mL^{-1} of melanin. Treatment with **9i**, on the contrary, decreased the melanin levels to 62 μg mL^{-1}, meaning that there was a significant reduction in melanin content as compared to the control groups, thus affirming that **9i** exhibits inhibitory potential to reduce melanin synthesis in B16F10 cells.

Table 3 Cytotoxicity evaluation of **9i** on the B16F10 cell line[a]

Concentration	% Viability ± SE[a]
200 μM	51.19 ± 4.34
150 μM	58.24 ± 3.43
100 μM	82.97 ± 5.31

[a] Data expressed as mean ± SE.

3. Conclusion

In this study, a series of novel aminomethyl 1,2,3-triazole–cinamamide hybrid compounds were synthesized and tested for their anti-tyrosinase, antioxidant, and anti-melanogenic effects. All compounds synthesized were screened for tyrosinase inhibition activity. The SAR investigations have evidenced that the substitution at R^1 and R^2 generally increases potency. Kinetic studies confirmed the competitive inhibition mechanism of **9i** with a K_i of 34.36 μM, whereby it binds to the active site of the enzyme. The compounds exhibited mild to good antioxidant activities when examined by DPPH radical scavenging assays, which would help alleviate oxidative stress typically associated with hyperpigmentation disorders. The anti-melanogenic potential of these compounds was further corroborated through their biological activities on the B16F10 murine melanoma cell line. In particular, compound **9i** significantly reduced melanin content to 62 μg mL^{-1} at 70 μM concentration compared with untreated controls. In contrast, the compound showed limited cytotoxicity, making it an ideal candidate for further drug development.

4. Method and materials

4.1 General procedure for the synthesis of 9a–q

A mixture of benzaldehyde derivatives (**1a–c**, 25 mmol), malonic acid (**2**, 25 mmol), pyridine (15 mL), and piperidine (5 mL) was stirred for 3 h at 100 °C. Thereafter, water (300 mL) was added, and the mixture was neutralized with concentrated HCl.[18] To a mixture of cinnamic acid derivatives **3a–c** (10 mmol) and

propargylamine **4** (10 mmol) in DMF (50 mL), TBTU (13 mmol) and Et_3N (13 mmol) were added, and the obtained mixture was stirred for 24 h at room temperature (rt). After completion of the reaction, water was added to this reaction mixture, and the precipitate was filtered to give pure *N*-(prop-2-yn-1-yl) cinnamamide derivatives **5a–c**.[19]

Aniline derivatives (**6a–e**, 50 mmol) were suspended in DMF (25 mL) and cooled to 0 °C. Next, chloroacetyl chloride (65 mmol) was added, and the reaction mixture was then stirred at room temperature for 24 h. At the end of the reaction, the reaction mixture was diluted with water, poured into crushed ice, and the resulting precipitates were filtered off. Finally, the residue was washed with water to obtain 2-chloro-*N*-substituted acetamide derivatives **7a–e**.[20,21] A mixture of acetamides **7a–o** (1.2 mmol), K_2CO_3 (1.5 mmol), and NaN_3 (1.5 mmol) in DMF was stirred at room temperature for 1 h. Then, copper sulfate pentahydrate ($CuSO4 \cdot 5H_2O$, 0.15 mmol), sodium ascorbate (0.45 mmol), and *N*-(prop-2-yn-1-yl)cinnamamide derivatives (**5a–c**, 1 mmol) were added to the reaction mixture. After the completion of the reaction, copper ions were removed from the reaction mixture using an EDTA (ethylenediaminetetraacetic acid) solution (0.05 M). Then, the resulting precipitate was filtered and washed several times with water and crystallized from ethyl acetate to obtain pure *N*-((1*H*-1,2,3-triazol-4-yl) methyl)cinnamamide-*N*-substituted acetamides **9a–q**.

4.1.1 *N*-((1-(2-Oxo-2-(phenylamino)ethyl)-1*H*-1,2,3-triazol-4-yl)methyl)cinnamamide (9a). Brown solid; yield: 89%; mp = 141–143 °C; IR (KBr, ν_{max}): 3295, 3010, 2935, 1658 cm^{-1}. ^1H NMR (300 MHz, DMSO-d_6): δ 10.51 (s, 1H, NH), 8.74 (t, J = 5.0 Hz, 1H, NH), 8.07 (s, 1H, triazole), 7.66–7.57 (m, 4H, Ar), 7.53 (d, J = 15.8 Hz, 1H, CH), 7.46–7.30 (m, 5H, Ar), 7.10 (t, J = 7.3 Hz, 1H, Ar), 6.74 (d, J = 15.8 Hz, 1H, CH), 5.36 (s, 2H, CH_2), 4.53 (d, J = 5.3 Hz, 2H, CH_2). ^{13}C NMR (75 MHz, DMSO-d_6): δ 165.4, 164.7, 145.3, 139.6, 138.9, 135.3, 132.3, 130.0, 129.4, 128.0, 125.2, 124.2, 122.4, 119.7, 52.7, 34.8. $C_{20}H_{19}N_5O_2$; calcd C, 66.47; H, 5.30; N, 19.38; found C, 66.62; H, 5.48; N, 19.56.

4.1.2 *N*-((1-(2-((4-Fluorophenyl)amino)-2-oxoethyl)-1*H*-1,2,3-triazol-4-yl)methyl)cinnamamide (9b). Brown solid; yield: 69%; mp = 168–170 °C; IR (KBr, ν_{max}): 3347, 3030, 2950, 1666 cm^{-1}. ^1H NMR (300 MHz, DMSO-d_6): δ 10.56 (s, 1H, NH), 8.73 (t, J = 5.5 Hz, 1H, NH), 8.05 (s, 1H, triazole), 7.67–7.56 (m, 4H, Ar), 7.52 (d, J = 15.8 Hz, 1H, CH), 7.47–7.37 (m, 3H, CH), 7.19 (t, J = 8.8 Hz, 2H, Ar), 6.73 (d, J = 15.8 Hz, 1H, CH), 5.35 (s, 2H, CH_2), 4.52 (d, J = 5.5 Hz, 2H, CH_2). ^{13}C NMR (75 MHz, DMSO-d_6): δ 165.4, 164.7, 158.7 (d, J = 240.3 Hz), 145.2, 139.5, 135.3, 135.2, 130.0, 129.4, 128.0, 125.1, 122.4, 121.5 (d, J = 7.9 Hz), 116.0 (d, J = 22.1 Hz), 52.58, 34.8. $C_{20}H_{18}FN_5O_2$; calcd C, 63.32; H, 4.78; N, 18.46; found C, 63.47; H, 4.93; N, 18.68.

4.1.3 *N*-((1-(2-((4-Chlorophenyl)amino)-2-oxoethyl)-1*H*-1,2,3-triazol-4-yl)methyl)cinnamamide (9c). Brown solid; yield: 78%; mp = 152–154 °C; IR (KBr, ν_{max}): 3320, 3035, 2955, 1664 cm^{-1}. ^1H NMR (300 MHz, DMSO-d_6): δ 10.63 (s, 1H, NH), 8.71 (t, J = 5.5 Hz, 1H, NH), 8.04 (s, 1H, triazole), 7.64 (d, J = 8.8 Hz, 2H, Ar), 7.61–7.55 (m, 2H, Ar), 7.50 (d, J = 15.8 Hz, 1H, CH), 7.47–7.33 (m, 5H, Ar), 6.72 (d, J = 15.8 Hz, 1H, CH), 5.35 (s, 2H, CH_2), 4.50 (d, J = 5.5 Hz, 2H, CH_2). ^{13}C NMR (75 MHz, DMSO-d_6): δ 165.4, 164.9, 145.2, 139.5, 137.9, 135.3, 130.0, 129.4, 129.3, 128.0, 127.8, 125.1, 122.4, 121.2, 52.6, 34.8. $C_{20}H_{18}ClN_5O_2$; calcd C, 60.69; H, 4.58; N, 17.69; found C, 60.86; H, 4.76; N, 17.89.

4.1.4 *N*-((1-(2-((4-Bromophenyl)amino)-2-oxoethyl)-1*H*-1,2,3-triazol-4-yl)methyl)cinnamamide (9d). Brown solid; yield: 65%; mp = 161–163 °C; IR (KBr, ν_{max}): 3334, 304, 2960, 1667 cm^{-1}. ^1H NMR (300 MHz, DMSO-d_6): δ 10.64 (s, 1H, NH), 8.72 (t, J = 4.8 Hz, 1H, NH), 8.05 (s, 1H, triazole), 7.61–7.51 (m, 6H, Ar), 7.50–7.36 (m, 4H, Ar, CH), 6.72 (d, J = 15.8 Hz, 1H, CH), 5.35 (s, 2H, CH_2), 4.50 (d, J = 4.8 Hz, 2H, CH_2). ^{13}C NMR (75 MHz, DMSO-d_6): δ 165.4, 165.0, 145.1, 139.5, 138.3, 135.3, 132.2, 130.0, 129.4, 128.0, 125.1, 122.4, 121.6, 115.9, 52.6, 34.8. $C_{20}H_{18}BrN_5O_2$; calcd C, 54.56; H, 4.12; N, 15.91; found C, 54.56; H, 4.12; N, 15.91.

4.1.5 *N*-((1-(2-((4-Ethylphenyl)amino)-2-oxoethyl)-1*H*-1,2,3-triazol-4-yl)methyl)cinnamamide (9e). Brown solid; yield: 68%; mp = 158–160 °C; IR (KBr, ν_{max}): 3311, 3020, 2950, 1663 cm^{-1}; ^1H NMR (300 MHz, DMSO-d_6): δ 10.44 (s, 1H, NH), 8.73 (t, J = 5.3 Hz, 1H, NH), 8.05 (s, 1H, triazole), 7.64–7.48 (m, 5H, Ar), 7.46–7.37 (m, 3H, Ar, CH), 7.18 (d, J = 7.5 Hz, 2H, Ar), 6.74 (d, J = 15.8 Hz, 1H, CH), 5.34 (s, 2H, CH_2), 4.52 (d, J = 5.3 Hz, 2H, CH_2), 2.57 (q, J = 7.4 Hz, 2H, CH_2), 1.17 (t, J = 7.4 Hz, 3H, CH_3). ^{13}C NMR (75 MHz, DMSO-d_6): δ 165.4, 164.5, 145.2, 139.7, 139.5, 136.6, 135.3, 130.0, 129.4, 128.6, 128.0, 125.1, 122.4, 119.8, 52.6, 34.8, 28.1, 16.1. $C_{22}H_{23}N_5O_2$; calcd C, 67.85; H, 5.95; N, 17.98; found C, 68.02; H, 6.12; N, 18.15.

4.1.6 3-(4-Chlorophenyl)-*N*-((1-(2-oxo-2-(phenylamino) ethyl)-1*H*-1,2,3-triazol-4-yl)methyl)acrylamide (9f). Brown solid; yield: 73%; mp = 163–165 °C; IR (KBr, ν_{max}): 3337, 3030, 2940, 1661 cm^{-1}. ^1H NMR (300 MHz, DMSO-d_6): δ 10.50 (s, 1H, NH), 8.74 (t, J = 5.3 Hz, 1H, NH), 8.05 (s, 1H, triazole), 7.64–7.57 (m, 4H, Ar), 7.54–7.45 (m, 3H, Ar, CH), 7.40–7.30 (m, 2H, Ar), 7.10 (t, J = 7.2 Hz, 1H, Ar), 6.73 (d, J = 15.8 Hz, 1H, CH), 5.35 (s, 2H, CH_2), 4.51 (d, J = 5.3 Hz, 2H, CH_2). ^{13}C NMR (75 MHz, DMSO-d_6) δ 165.2, 164.7, 145.0, 138.9, 138.2, 134.4, 134.3, 129.7, 129.4, 129.4, 125.1, 124.3, 123.1, 119.7, 52.6, 34.8. $C_{20}H_{18}ClN_5O_2$; calcd C, 60.69; H, 4.58; N, 17.69; found C, 60.78; H, 4.70; N, 17.91.

4.1.7 3-(4-Chlorophenyl)-*N*-((1-(2-((4-fluorophenyl)amino)-2-oxoethyl)-1*H*-1,2,3-triazol-4-yl)methyl)acrylamide (9g). Brown solid; yield: 60%; mp = 185–187 °C; IR (KBr, ν_{max}): 3351, 3025, 2965, 1668 cm^{-1}. ^1H NMR (300 MHz, DMSO-d_6): δ 10.56 (s, 1H, NH), 8.73 (t, J = 5.0 Hz, 1H, NH), 8.05 (s, 1H, triazole), 7.71–7.57 (m, 4H, Ar), 7.54–7.40 (m, 3H, Ar, CH), 7.23–7.11 (m, 2H, Ar), 6.72 (d, J = 15.8 Hz, 1H, CH), 5.34 (s, 2H, CH_2), 4.51 (d, J = 5.0 Hz, 2H, CH_2). ^{13}C NMR (76 MHz, DMSO-d_6): δ 165.2, 164.7, 158.7 (d, J = 240.3 Hz), 145.0, 138.2, 135.3, 134.3 (d, J = 9.3 Hz), 129.7, 129.4, 125.1, 123.2, 121.5, 121.4, 116.0 (d, J = 22.1 Hz), 52.6, 34.8. $C_{20}H_{17}ClFN_5O_2$; calcd C, 58.05; H, 4.14; N, 16.92; found C, 58.19; H, 4.31; N, 17.10.

4.1.8 3-(4-Chlorophenyl)-*N*-((1-(2-((4-chlorophenyl)amino)-2-oxoethyl)-1*H*-1,2,3-triazol-4-yl)methyl)acrylamide (9h). Brown solid; yield: 58%; mp = 174–1176 °C; IR (KBr, ν_{max}): 3342, 3055, 2945, 1667 cm^{-1}. ^1H NMR (300 MHz, DMSO-d_6): δ 10.64 (s, 1H, NH), 8.74 (t, J = 5.2 Hz, 1H, NH), 8.04 (s, 1H, triazole), 7.66–7.58 (m, 4H, Ar), 7.54–7.45 (m, 3H, Ar, CH), 7.40 (d, J = 8.7 Hz, 2H, Ar), 6.72 (d, J = 15.8 Hz, 1H, CH), 5.35 (s, 2H, CH_2), 4.50 (d, J = 5.2 Hz, 2H, CH_2). ^{13}C NMR (75 MHz, DMSO-d_6): δ 165.2, 164.9,

145.2, 138.2, 137.8, 134.4, 134.3, 129.7, 129.4, 129.3, 127.9, 125.2, 123.1, 121.3, 52.6, 34.8. $C_{20}H_{17}C_{l2}N_5O_2$; calcd C, 55.83; H, 3.98; N, 16.28; found C, 55.98; H, 4.16; N, 16.39.

4.1.9 *N*-((1-(2-((4-Bromophenyl)amino)-2-oxoethyl)-1*H*-1,2,3-triazol-4-yl)methyl)-3-(4-chlorophenyl)acrylamide (9i). Brown solid; yield: 61%; mp = 161–163 °C; IR (KBr, ν_{max}): 3352, 3060, 2935, 1665 cm^{-1}. ^1H NMR (300 MHz, DMSO-d_6): δ 10.63 (s, 1H, NH), 8.73 (t, J = 5.0 Hz, 1H, NH), 8.03 (s, 1H, triazole), 7.63–7.58 (m, 3H, Ar), 7.57–7.53 (m, 3H, Ar), 7.52–7.45 (m, 3H, Ar, CH), 6.71 (d, J = 15.8 Hz, 1H, CH), 5.34 (s, 2H, CH_2), 4.49 (d, J = 5.0 Hz, 2H, CH_2). ^{13}C NMR (75 MHz, DMSO-d_6): δ 165.2, 164.9, 145.1, 138.2, 138.2, 134.4, 134.3, 132.2, 129.7, 129.5, 125.1, 123.2, 121.6, 115.9, 52.6, 34.8. $C_{20}H_{17}BrClN_5O_2$; calcd C, 50.60; H, 3.61; N, 14.75; found C, 50.74; H, 3.82; N, 14.88. The purity of the compound was checked using HPLC.

4.1.10 3-(4-Chlorophenyl)-*N*-((1-(2-((4-ethylphenyl)amino)-2-oxoethyl)-1*H*-1,2,3-triazol-4-yl)methyl)acrylamide (9j). Brown solid; yield: 59%; mp = 172–174 °C; IR (KBr, ν_{max}): 3322, 3040, 2965, 1668 cm^{-1}. ^1H NMR (300 MHz, DMSO-d_6): δ 10.41 (s, 1H, NH), 8.73 (t, J = 5.4 Hz, 1H, NH), 8.04 (s, 1H, triazole), 7.61 (d, J = 8.5 Hz, 2H, Ar), 7.56–7.45 (m, 5H, Ar, CH), 7.17 (d, J = 8.5 Hz, 2H, Ar), 6.73 (d, J = 15.8 Hz, 1H, CH), 5.33 (s, 2H, CH_2), 4.51 (d, J = 5.4 Hz, 2H, CH_2), 2.55 (q, J = 7.6 Hz, 2H, CH_2), 1.16 (t, J = 7.6 Hz, 3H, CH_3). ^{13}C NMR (75 MHz, DMSO-d_6): δ 165.2, 164.5, 145.0, 139.6, 138.2, 136.6, 134.4, 134.3, 129.7, 129.4, 128.6, 125.1, 123.2, 119.8, 52.63, 34.82, 28.07, 16.10. $C_{22}H_{22}ClN_5O_2$; calcd C, 62.34; H, 5.23; N, 16.52; found C, 62.51; H, 5.38; N, 16.73.

4.1.11 3-(4-Chlorophenyl)-*N*-((1-(2-((4-methoxyphenyl)amino)-2-oxoethyl)-1*H*-1,2,3-triazol-4-yl)methyl)acrylamide (9k). Brown solid; yield: 79%; mp = 182–184 °C; IR (KBr, ν_{max}): 3336, 3015, 2970, 1673 cm^{-1}. ^1H NMR (400 MHz, DMSO-d_6) δ 10.34 (s, 1H, NH), 8.71 (t, J = 5.8 Hz, 1H, NH), 8.01 (s, 1H, triazole), 7.60 (d, J = 8.5 Hz, 2H, Ar), 7.53–7.42 (m, 5H, Ar, CH), 6.91 (d, J = 9.0 Hz, 2H, Ar), 6.70 (d, J = 15.8 Hz, 1H, CH), 5.28 (s, 2H, CH_2), 4.48 (d, J = 5.8 Hz, 2H, CH_2), 3.72 (s, 3H, OCH_3). ^{13}C NMR (100 MHz, DMSO-d_6) δ 165.1, 164.2, 156.0, 145.0, 138.2, 134.4, 134.3, 132.0, 129.7, 129.5, 125.1, 123.2, 121.2, 114.5, 55.6, 52.5, 34.8. $C_{21}H_{20}ClN_5O_3$; calcd C, 59.23; H, 4.73; N, 16.45; found C, 59.47; H, 4.88; N, 16.59.

4.1.12 3-(4-Methoxyphenyl)-*N*-((1-(2-oxo-2-(phenylamino)ethyl)-1*H*-1,2,3-triazol-4-yl)methyl)acrylamide (9l). Brown solid; yield: 81%; mp = 159–161 °C; IR (KBr, ν_{max}): 3319, 3045, 2950, 1670 cm^{-1}. ^1H NMR (300 MHz, DMSO-d_6): δ 10.52 (s, 1H, NH), 8.64 (t, J = 5.0 Hz, 1H, NH), 8.05 (s, 1H, triazole), 7.62 (d, J = 7.5 Hz, 2H, Ar), 7.54 (d, J = 8.4 Hz, 2H, Ar), 7.47 (d, J = 15.7 Hz, 1H, CH), 7.35 (t, J = 7.5 Hz, 2H, Ar), 7.10 (t, J = 7.5 Hz, 1H, Ar), 6.99 (d, J = 8.4 Hz, 2H, Ar), 6.59 (d, J = 15.7 Hz, 1H, CH), 5.36 (s, 2H, CH_2), 4.51 (d, J = 5.0 Hz, 2H, CH_2), 3.79 (s, 3H, OCH_3). ^{13}C NMR (75 MHz, DMSO-d_6): δ 165.7, 164.7, 160.8, 145.2, 139.2, 138.9, 129.6, 129.4, 127.9, 125.1, 124.2, 119.9, 119.7, 114.9, 55.7, 52.7, 34.8. $C_{21}H_{21}N_5O_3$; calcd C, 64.44; H, 5.41; N, 17.89; found C, 64.57; H, 5.64; N, 18.07.

4.1.13 *N*-((1-(2-((4-Fluorophenyl)amino)-2-oxoethyl)-1*H*-1,2,3-triazol-4-yl)methyl)-3-(4-methoxyphenyl)acrylamide (9m). Brown solid; yield: 56%; mp = 187–189 °C; IR (KBr, ν_{max}): 3337, 3055, 2965, 1668 cm^{-1}. ^1H NMR (300 MHz, DMSO-d_6): δ 10.58 (s, 1H, NH), 8.63 (t, J = 5.0 Hz, 1H, NH), 8.04 (s, 1H, triazole), 7.69–7.59 (m, 3H, Ar), 7.53 (d, J = 8.5 Hz, 2H, Ar), 7.46 (d, J = 15.7 Hz, 1H, CH), 7.19 (t, J = 8.7 Hz, 2H, Ar), 6.99 (d, J = 8.5 Hz, 2H, Ar), 6.58 (d, J = 15.8 Hz, 1H, CH), 5.35 (s, 2H, CH_2), 4.50 (d, J = 5.0 Hz, 2H, CH_2), 3.79 (s, 3H, OCH_3). ^{13}C NMR (75 MHz, DMSO-d_6): δ 165.7, 164.7, 160.8, 158.7 (d, J = 240.4 Hz), 145.2, 139.2, 135.3 (d, J = 2.5 Hz), 129.6, 127.9, 125.1, 121.5, 119.9, 116.0 (d, J = 22.1 Hz), 114.8, 55.69, 52.58, 34.78. $C_{21}H_{20}FN_5O_3$; calcd C, 61.61; H, 4.92; N, 17.11; found C, 61.78; H, 5.09; N, 17.34.

4.1.14 *N*-((1-(2-((4-Chlorophenyl)amino)-2-oxoethyl)-1*H*-1,2,3-triazol-4-yl)methyl)-3-(4-methoxyphenyl)acrylamide (9n). Brown solid; yield: 68%; mp = 179–181 °C; IR (KBr, ν_{max}): 3338, 3020, 2960, 1671 cm^{-1}. ^1H NMR (300 MHz, DMSO-d_6): δ 10.64 (s, 1H, NH), 8.63 (t, J = 5.4 Hz, 1H, NH), 8.05 (s, 1H, triazole), 7.64 (d, J = 8.8 Hz, 2H), 7.53 (d, J = 8.6 Hz, 2H), 7.47 (d, J = 15.8 Hz, 1H), 7.40 (d, J = 8.8 Hz, 2H), 6.98 (d, J = 8.6 Hz, 2H), 6.58 (d, J = 15.8 Hz, 1H), 5.36 (s, 2H, CH_2), 4.51 (d, J = 5.4 Hz, 2H, CH_2), 3.79 (s, 3H, OCH_3). ^{13}C NMR (75 MHz, DMSO-d_6): δ 165.8, 164.9, 160.8, 145.3, 139.3, 137.8, 131.9, 129.6, 129.3, 127.9, 125.1, 121.3, 119.9, 114.8, 55.7, 52.6, 34.8. $C_{21}H_{20}ClN_5O_3$; calcd C, 59.23; H, 4.73; N, 16.45; found C, 59.48; H, 4.86; N, 16.61.

4.1.15 *N*-((1-(2-((4-Bromophenyl)amino)-2-oxoethyl)-1*H*-1,2,3-triazol-4-yl)methyl)-3-(4-methoxyphenyl)acrylamide (9o). Brown solid; yield: 68%; mp = 180–182 °C; IR (KBr, ν_{max}): 3349, 3065, 2935, 1674 cm^{-1}. ^1H NMR (300 MHz, DMSO-d_6): δ 10.63 (s, 1H, NH), 8.61 (t, J = 5.6 Hz, 1H, NH), 8.03 (s, 1H, triazole), 7.62–7.50 (m, 6H, Ar), 7.46 (d, J = 15.8 Hz, 1H, CH), 6.99 (d, J = 8.7 Hz, 2H, Ar), 6.57 (d, J = 15.8 Hz, 1H, CH), 5.35 (s, 2H, CH_2), 4.50 (d, J = 5.6 Hz, 2H, CH_2), 3.80 (s, 3H, OCH_3). ^{13}C NMR (75 MHz, DMSO-d_6): δ 165.7, 165.0, 160.8, 145.2, 139.2, 138.2, 132.2, 129.6, 127.9, 125.1, 121.6, 119.9, 115.9, 114.9, 55.7, 52.6, 34.8. $C_{21}H_{20}BrN_5O_3$; calcd C, 53.63; H, 4.29; N, 14.89; found C, 53.78; H, 4.46; N, 15.04.

4.1.16 *N*-((1-(2-((4-Ethylphenyl)amino)-2-oxoethyl)-1*H*-1,2,3-triazol-4-yl)methyl)-3-(4 methoxyphenyl)acrylamide (9p). Brown solid; yield: 74%; mp = 166–168 °C; IR (KBr, ν_{max}): 3333, 3050, 2935, 1669 cm^{-1}. ^1H NMR (300 MHz, DMSO-d_6): δ 10.44 (s, 1H, NH), 8.64 (t, J = 5.3 Hz, 1H, NH), 8.05 (s, 1H, triazole), 7.59–7.41 (m, 5H, Ar, CH), 7.17 (d, J = 7.8 Hz, 2H, Ar), 6.99 (d, J = 8.1 Hz, 2H, Ar), 6.60 (d, J = 15.7 Hz, 1H, CH), 5.34 (s, 2H, CH_2), 4.51 (d, J = 5.3 Hz, 2H, CH_2), 3.79 (s, 3H, OCH_3), 2.55 (q = 7.5 Hz, 2H, CH_2), 1.16 (t, J = 7.5 Hz, 3H, CH_3). ^{13}C NMR (75 MHz, DMSO-d_6): δ 165.7, 164.5, 160.8, 145.2, 139.7, 139.3, 136.6, 129.6, 128.6, 127.9, 125.1, 119.9, 119.8, 114.4, 55.7, 52.6, 34.8, 28.1, 16.1. $C_{23}H_{25}N_5O_3$; calcd C, 65.86; H, 6.01; N, 16.70; found C, 66.03; H, 6.17; N, 16.91.

4.1.17 3-(4-Methoxyphenyl)-*N*-((1-(2-((4-methoxyphenyl)amino)-2-oxoethyl)-1*H*-1,2,3-triazol-4-yl)methyl)acrylamide (9q). Brown solid; yield: 87%; mp = 173–175 °C; IR (KBr, ν_{max}): 3324, 3032, 2945, 1670 cm^{-1}. ^1H NMR (400 MHz, DMSO-d_6) δ 10.34 (s, 1H, NH), 8.59 (t, J = 5.8 Hz, 1H, NH), 8.00 (s, 1H, triazole), 7.57–7.48 (m, 4H, Ar), 7.43 (d, J = 15.8 Hz, 1H, CH), 6.98 (d, J = 8.5 Hz, 2H, Ar), 6.91 (d, J = 9.1 Hz, 2H, Ar), 6.55 (d, J = 15.7 Hz, 1H, CH), 5.28 (s, 2H, CH_2), 4.47 (d, J = 5.7 Hz, 2H, CH_2), 3.78 (s, 3H, OCH_3), 3.72 (s, 3H, OCH_3). ^{13}C NMR (100 MHz, DMSO-d_6) δ 165.7, 164.2, 160.8, 156.0, 145.2, 139.2, 132.0, 129.6, 127.9, 125.0, 121.2, 119.9, 114.8, 114.5, 55.7, 55.6, 52.5,

34.7. $C_{22}H_{23}N_5O_4$; calcd C, 62.70; H, 5.50; N, 16.62; found C, 63.03; H, 5.65; N, 16.81. MS ES$^+$: *m*/*z* 442.2910 $[M + 1]^+$ and 445.2930 $[M + 23]^+$.

4.2 Tyrosinase inhibitory assay

The tyrosinase activity assay for compounds followed a modified procedure. In brief, in a 96-well microplate, 160 μL of phosphate buffer (50 mM, pH = 6.8), 10 μL of lyophilized mushroom tyrosinase powder (CAS no. 9002-10-2 dissolved in water with 500 units per mg), and 10 μL of the test compound (dissolved in DMSO) were added. Subsequently, 20 μL of L-DOPA (dissolved in water) was added to initiate the enzymatic reaction. The change in absorbance at 475 nm was continuously monitored using a spectrophotometer. DMSO without test compounds served as the control, while kojic acid acted as the positive control.[22,23]

4.3 Determination of the inhibition type

The most potent derivative was selected for kinetic analysis, and its inhibitory activity was assessed at different inhibitor concentrations. The substrate (L-DOPA) concentrations ranged from 0.5 to 2.8 mM according to the previously reported procedures.[24]

4.4 Free radical-scavenging activity evaluation

As described previously, radical-scavenging activity was assessed using the 2,2-diphenyl-1-picrylhydrazyl (DPPH) assay. Briefly, the mixture of different concentrations of the compounds and DPPH methanolic solution (110 μM) was shaken in the dark at room temperature for 30 min. The mixture absorbance was measured at 517 nm. Quercetin was used as the positive control.[25]

4.5 Molecular docking study

Docking analysis was conducted to elucidate the interaction modes of the designed molecules with the tyrosinase enzyme. The Maestro Molecular Modeling by Schrödinger was utilized for this purpose. The X-ray crystal structure of the receptor (PDB ID: 2Y9X), with tropolone, was extracted from the Protein Data Bank. Before docking, protein preparation involved the removal of the native ligand and water molecules, followed by the addition of hydrogen atoms, with nonpolar hydrogens subsequently merged. The 2D structures of all synthesized compounds were drawn using the Marvin program, and their 3D structures were generated and optimized using LigPrep.[26]

4.6 Molecular dynamics simulation

MD simulation was conducted using Desmond v5.3 (part of the Schrödinger 2018-4 suite) on the best pose of the **9i** complex extracted from induced fit docking.[27]

4.7 MTT assay for cell viability

The cytotoxic activity of all derivatives was determined using the 3-(4,5-dimethylthiazol-2-yl)-2,5-diphenyltetrazolium bromide (MTT) assay. B16F10 were obtained from the Pasteur Institute of Iran (https://en.pasteur.ac.ir/). Cells (at a density of 25 000 cells per ml) were grown at 37 °C in the presence of CO_2 5% in DMEM (Gibco BRL, Grand Island, NY, USA), 10% fetal bovine serum (FBS, Gibco BRL). Next, cells were seeded in a 96-well plate and incubated at 37 °C with the derivative at different concentrations for 72 h. Following treatment, cells were incubated with MTT (0.5 mg mL^{-1}) for 3 h. The MTT-containing medium was then removed, and 100 μL of DMSO was added to each well, mixed thoroughly with a 10-minute shake to dissolve the formazan crystals. The absorbance of each well was measured at 540 nm.[28]

4.8 Determination of melanin content

The melanin content assay was performed according to previously reported protocols with minor modifications. Briefly, B16F10 cells were seeded in 12-well plates at a density of 50 000 cells per well. After 24 hours of incubation, 100 nM α-MSH was added to each well, followed by the addition of compound **9i** five hours later. The plates were then incubated for an additional 48 hours. Subsequently, the cells were washed twice with PBS and harvested using 0.25 M trypsin. The cell pellets were dissolved in 200 μL of 1 N NaOH containing 10% DMSO and incubated at 80 °C for 2 hours to solubilize the melanin. The absorbance of the resulting supernatant was measured at 470 nm using a microplate reader. The melanin content was quantified using a calibration curve constructed from synthetic melanin standards, measured at 405 nm. Kojic acid was used as a positive control for comparison.[29]

Conflicts of interest

There are no conflicts to declare.

Data availability

The datasets generated and/or analyzed during the current study are available in the Worldwide Protein Data Bank under the PDB ID 2Y9X (https://www.rcsb.org/structure/2Y9X). The NMR and spectral data are provided in the supplementary information (SI). Supplementary information is available. See DOI: https://doi.org/10.1039/d5ra04315h.

Acknowledgements

The authors wish to thank the financial support of the Vice-Chancellor for Research of Shiraz University of Medical Sciences, with grant number IR.SUMS.REC.1404.117.

References

1 M. Pretzler and A. Rompel, Tyrosinases: a family of copper-containing metalloenzymes, *ChemTexts*, 2024, **10**(4), 12.
2 L. J. Opperman, *The Phenomenon of Skin Lightening Among Young Adults, and the Effect of Selected Plant Extracts on Tyrosinase and Melanogenesis Activity*, University of the Western Cape, 2023.

3 F. Liu, *et al.*, Advances in biomedical functions of natural whitening substances in the treatment of skin pigmentation diseases, *Pharmaceutics*, 2022, **14**(11), 2308.
4 W. Jin, *et al.*, Dysregulation of tyrosinase activity: a potential link between skin disorders and neurodegeneration, *J. Pharm. Pharmacol.*, 2024, **76**(1), 13–22.
5 B. Singh, *et al.*, Enzymatic browning of fruit and vegetables: A review, *Enzymes in Food Technology: Improvements and Innovations*, 2018, pp. 63–78.
6 P. Rasane, *et al.*, Strategic advances in the management of browning in fruits and vegetables, *Food Bioprocess Technol.*, 2024, **17**(2), 325–350.
7 T. Takahashi and M. Miyazawa, Tyrosinase inhibitory activities of cinnamic acid analogues, *Pharmazie*, 2010, **65**(12), 913–918.
8 Y. C. Boo, Coumaric Acid as An Active Ingredient in Cosmetics: A Review Focusing on its Antimelanogenic Effects, *Antioxidants*, 2019, **8**(8), 275.
9 H. S. Yoon, *et al.*, Differential effects of methoxylated p-coumaric acids on melanoma in B16/F10 cells, *Prev. Nutr. Food Sci.*, 2015, **20**(1), 73.
10 K. Iwai, *et al.*, In Vitro Antioxidative Effects and Tyrosinase Inhibitory Activities of Seven Hydroxycinnamoyl Derivatives in Green Coffee Beans, *J. Agric. Food Chem.*, 2004, **52**(15), 4893–4898.
11 A. Mermer and S. Demirci, Recent advances in triazoles as tyrosinase inhibitors, *Eur. J. Med. Chem.*, 2023, **259**, 115655.
12 S. Vittorio, C. Dank and L. Ielo, Heterocyclic Compounds as Synthetic Tyrosinase Inhibitors: Recent Advances, *Int. J. Mol. Sci.*, 2023, **24**(10), 9097.
13 M. Ashooriha, *et al.*, 1,2,3-Triazole-based kojic acid analogs as potent tyrosinase inhibitors: Design, synthesis and biological evaluation, *Bioorg. Chem.*, 2019, **82**, 414–422.
14 M. Mahdavi, *et al.*, Synthesis of New Benzimidazole-1,2,3-triazole Hybrids as Tyrosinase Inhibitors, *Chem. Biodiversity*, 2018, **15**(7), e1800120.
15 M. Divar, *et al.*, Benzyl-Triazole Derivatives of Hydrazinecarbothiamide Derivatives as Potent Tyrosinase Inhibitors: Synthesis, Biological Evaluation, Structure-Activity Relationship and Docking Study, *ChemistrySelect*, 2023, **8**(8), e202203382.
16 A. S. Shokouhi Asl, *et al.*, Cinnamic acid conjugated with triazole acetamides as anti-Alzheimer and anti-melanogenesis candidates: an in vitro and in silico study, *Sci. Rep.*, 2025, **15**(1), 655.
17 V. V. Rostovtsev, *et al.*, A stepwise huisgen cycloaddition process: copper(I)-catalyzed regioselective "ligation" of azides and terminal alkynes, *Angew Chem. Int. Ed. Engl.*, 2002, **41**(14), 2596–2599.
18 W. Starflinger, G. Kresze and K. Huss, Ene reaction mechanisms. 3. Intermolecular and intramolecular kinetic isotope effects (KIE) for some ene reactions of hetero enophiles, *J. Inorg. Chem.*, 1986, **51**(1), 37–40.
19 M. H. Sayahi, *et al.*, Design, synthesis, in vitro, and in silico anti-α-glucosidase assays of N-phenylacetamide-1,2,3-triazole-indole-2-carboxamide derivatives as new anti-diabetic agents, *Sci. Rep.*, 2024, **14**(1), 15791.
20 F. Yousefnejad, *et al.*, Design, synthesis, in vitro, and in silico evaluations of benzo [d] imidazole-amide-1, 2, 3-triazole-N-arylacetamide hybrids as new antidiabetic agents targeting α-glucosidase, *Sci. Rep.*, 2023, **13**(1), 12397.
21 M. Noori, *et al.*, Design, synthesis, and in silico studies of quinoline-based-benzo [d] imidazole bearing different acetamide derivatives as potent α-glucosidase inhibitors, *Sci. Rep.*, 2022, **12**(1), 14019.
22 A. Iraji, *et al.*, Design, synthesis, spectroscopic characterization, in vitro tyrosinase inhibition, antioxidant evaluation, in silico and kinetic studies of substituted indole-carbohydrazides, *Bioorg. Chem.*, 2022, **129**, 106140.
23 N. Motamedi Shakib, *et al.*, Development of mercapto-phenyl-1, 2, 4-triazole bearing thio-quinoline as a novel class of tyrosinase inhibitors: an in vitro and in silico study, *Sci. Rep.*, 2025, **15**(1), 25382.
24 S. Karimian, *et al.*, Design, synthesis, and biological evaluation of symmetrical azine derivatives as novel tyrosinase inhibitors, *BMC Chem.*, 2021, **15**(1), 54.
25 S. Moghadam Farid, *et al.*, Synthesis, biological evaluations, and in silico assessments of phenylamino quinazolinones as tyrosinase inhibitors, *Sci. Rep.*, 2025, **15**(1), 846.
26 A. Bagheri, *et al.*, Structure-based development of 3,5-dihydroxybenzoyl-hydrazineylidene as tyrosinase inhibitor; in vitro and in silico study, *Sci. Rep.*, 2024, **14**(1), 1540.
27 Z. Najafi, *et al.*, Design, synthesis, and molecular dynamics simulation studies of some novel kojic acid fused 2-amino-3-cyano-4H-pyran derivatives as tyrosinase inhibitors, *BMC Chem.*, 2024, **18**(1), 41.
28 M. Noori, *et al.*, Phenyl-quinoline derivatives as lead structure of cholinesterase inhibitors with potency to reduce the GSK-3β level targeting Alzheimer's disease, *Int. J. Biol. Macromol.*, 2023, **253**(Pt 7), 127392.
29 M. Noori, *et al.*, Thioquinoline derivatives conjugated to thiosemicarbazide as potent tyrosinase inhibitors with anti-melanogenesis properties, *Sci. Rep.*, 2023, **13**(1), 2578.